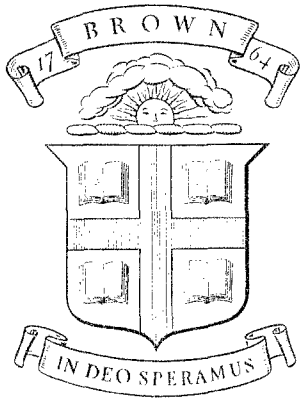

Division of Engineering
BROWN UNIVERSITY
PROVIDENCE, R. I.

HERTZIAN FRACTURE IN SINGLE CRYSTALS WITH THE DIAMOND STRUCTURE

B. R. LAWN

Department of Defense
Advanced Research Projects Agency
Contract SD-86
Materials Research Program

Industrial Distributors Ltd.

ARPA E40

May 1967

HERTZIAN FRACTURE IN SINGLE CRYSTALS WITH THE DIAMOND STRUCTURE

by

Brian R. Lawn

Division of Engineering
Brown University
Providence
Rhode Island

May 1967

Research supported by a grant from Industrial Distributors and by ARPA Contract E65.

ABSTRACT

Extension of an earlier theory of Hertzian fracture in brittle isotropic materials (Frank & Lawn 1967) is here made to include the case of brittle single crystals. A criterion is first proposed for predicting the path of a crack through an inhomogeneously stressed crystal in terms of the surface energy anisotropy of the crystal and the stresses prior to fracture occurring. This criterion is then applied to determine the geometry of cracks formed in the Hertzian stress field in crystals having the diamond structure. The computed crack geometries agree well with observation. An analysis of the fracture mechanics of crack growth into the crystal subsequently indicates that for a certain range of indenter size the Hertzian crack passes through four equilibrium stages, as it does in glass, before reaching its fully developed length. As a result Auerbach's law holds, i.e. the critical load on the indenter necessary to produce a fully developed Hertzian fracture is proportional to the radius of the indenter. This law is confirmed by Hertzian fracture tests on silicon single crystals. Finally, possible application of the Hertzian test to the study of some mechanical properties, such as fatigue, of brittle single crystals is indicated.

HERTZIAN FRACTURE IN SINGLE CRYSTALS WITH THE DIAMOND STRUCTURE

1. INTRODUCTION

In recent papers (Frank & Lawn 1967, Lawn 1967) the geometry and mechanics of Hertzian fracture in brittle, isotropic materials was treated in detail. In particular, a derivation of the long-established empirical Auerbach law (Auerbach 1891) was presented. This law states that the critical load P_c required for a hard, spherical indenter to produce a cone crack in a flat, brittle specimen is proportional to the radius r of the indenter. Interest stems from the fact that the theoretical analysis predicts that the constant of proportionality is linearly dependent on γ, a term often described as "the work of fracture" which, for ideally brittle materials, is simply the free energy required to create unit area of surface. Auerbach's law therefore affords a simple means of measuring γ in a relative manner under conditions of stable crack growth.

The investigation of Hertzian fracture mechanisms in single crystals with anisotropic surface energies and elastic moduli is of interest for the following reasons. Firstly, because of recent widespread activity in measurements of the γ term in single crystals it is desirable to establish the conditions (if any) under which Auerbach's law may be applicable. For instance it was noted (Lawn 1967) that the introduction of a sliding motion to the loaded indenter causes a sufficiently large perturbing effect on the stress field in the specimen

(even when the coefficient of friction between indenter and specimen is small) to destroy the Auerbach behaviour; it might be the case that the anisotropic nature of the specimen has a similar modifying effect. Secondly, the phenomenon of fracture in non-isotropic materials is itself a problem of great interest. The effect of anisotropy in $\underline{\gamma}$ and (if important) in the elastic constants of the specimen material on fracture is not well understood, most attention to crack-extension problems being directed toward isotropic cases. That crystallographic anisotropy does play a significant role in Hertzian fracture may be deduced from the observations of Howes & Tolansky on diamond (for a review see Howes 1965): the fracture geometry and critical fracture load $\underline{P}_c$ are both very much dependent on the crystallographic orientation of the diamond surface. To understand these effects one must investigate in some detail the basic mechanisms of crack extension in brittle materials. Difficulties arise in this more general case which are not made evident in the studies of cracks in isotropic bodies.

In the treatment which follows most of the principles will be applicable to single crystals in general. However, crystals possessing the diamond structure will be cited as particular examples for study since they are nominally brittle at room temperatures and $\underline{\gamma}$ is therefore determined principally by the reversible fracture surface energy; also, as will be discussed in §3, the variation of $\underline{\gamma}$ with crystallographic orientation is sufficiently well known. Further, although these materials exhibit elastic anisotropy it is not large. (The anisotropy factor $2\underline{c}_{44}/(\underline{c}_{11} - \underline{c}_{12})$ is, using the elastic constants quoted by Huntington (1958), of the order 1.3-1.5 which is

not as large as that for most metals.) It is therefore unlikely that anisotropy in the elastic constants will play as important a role in determining fracture paths as will anisotropy in surface energy. For the present it is simply pointed out that ignoring elastic anisotropy will lead to considerable reduction in mathematical computation. Finally, because of the demand for high quality semiconductor materials, large single crystals of silicon and germanium are readily obtainable commercially: complications due to microstructure and lattice imperfection do not arise.

2. CRACK EXTENSION THROUGH INHOMOGENEOUS STRESS FIELDS IN SINGLE CRYSTALS

2.1 Criterion for Crack Extension

To predict crack paths through an inhomogeneous stress field in any material it is necessary to consider the stress state at the crack tip. With regard to brittle isotropic materials Frank & Lawn (1967) began with the assumption of Griffith (1924) that a crack extends from that place at or adjacent to its tip where the local tangential tensile stress is a maximum. The crack increment therefore experiences zero shear stress, and it can thereby be concluded that the crack would tend to follow a surface delineated by the two lesser of the three principal stresses. This "maximum crack tip stress" criterion has been used to predict directions of extension of straight cracks in plexiglass plates subjected to plane loading (Erdogan & Sih 1963). The implication drawn from these studies is that such a criterion appears to be in

accord with an energy balance criterion, (i.e.) the predicted direction of crack growth appears to be that which releases the greatest amount of mechanical energy.

In going over to anisotropic materials (again treating only anisotropy in $\underline{\gamma}$ and ignoring that in the elastic constants) it soon becomes clear that the criterion outlined above is no longer applicable. This may be illustrated by referring to a hypothetical example. We consider a material which is relatively weak across one particular set of crystallographic planes and effectively infinitely strong across all others. (This picture applies reasonably well to "layer structures" such as mica.) The material is supposed to contain a crack not oriented along the plane of weakness, and is subsequently loaded until this crack is made to extend. Since the crack can only grow along the weak plane it follows that, when the loading is arbitrary, the location at the tip contour where the crack extends is <u>not</u> that where the local tensile stress is a maximum (except, of course, by sheer coincidence). The incremental extension of the crack then suffers both tensile ($\underline{T}_\theta$) and shear ($\underline{S}_{r\theta}$) stresses (figure 1) which may be determined by stress analysis. For instance, using polar coordinates, we have for a plane crack (Williams 1957)

$$T_\theta = \frac{1}{(2r)^{1/2}} \cos\frac{\theta}{2} \{K_\sigma \cos^2\frac{\theta}{2} - \frac{3}{2} K_\tau \sin\theta\}$$

$$S_{r\theta} = \frac{1}{(2r)^{1/2}} \frac{1}{2} \cos\frac{\theta}{2} \{K_\sigma \sin\theta + K_\tau(3\cos\theta - 1)\} \qquad (2.1)$$

where the $\underline{K}$ terms, the <u>stress intensity factors</u> (fracture mechanics notation), for a surface crack in a semi-infinite medium are given by

$$K_\sigma = \frac{2.24}{\pi} c^{\frac{1}{2}} \int_o^c \frac{\sigma(b)db}{(c^2-b^2)^{1/2}}$$

$$K_\tau = \frac{2.24}{\pi} c^{\frac{1}{2}} \int_o^c \frac{\tau(b)db}{(c^2-b^2)^{1/2}} . \qquad (2.2)$$

Here $\underline{c}$ is the crack length, $\underline{b}$ is the distance measured along the ultimate crack path, and $\underline{\sigma}(\underline{b})$ and $\underline{\tau}(\underline{b})$ are the prior normal and shear stresses along the crack path. Thus in the general case of a material having anisotropy in $\underline{\gamma}$ we conclude that a crack will extend at its tip in a direction other than that of maximum $\underline{T}_\theta$, and will subsequently be subjected to shear stresses along its path (that is, it will no longer follow the stress trajectories). With this in mind we are, therefore, obliged to reconsider the maximum crack tip tensile stress criterion for fracture growth, and to take special note of any influence the shear stress $\underline{S}_{r\theta}$ may have on this growth.

Up to this point we have treated the crack as though it were a deformed cut in a pefectly elastic material. Such a model allows one to postulate that the faces of an equilibrium crack (i.e. a crack whose length increases with an incremental increase in load) are stress free, an assumption greatly simplifying stress analysis. In reality, for materials such as crystals this model is not strictly correct. Molecular forces of cohesion act across the crack interface and modify the stresses and strains around the crack. The effect of cohesive forces has been discussed at length by Barenblatt (1962), and his approach to the problem will be adopted here. This will permit us to visualize possible effects of the shear stress $\underline{S}_{r\theta}$ on the incremental extension of the crack.

We consider first the contour of an equilibrium plane crack,

shown schematically in figure 2. According to Barenblatt the crack extends when the molecular forces of cohesion reach their highest possible intensity at some point on the crack tip contour. Since the cohesive forces rise to a very large maximum at an interplanar separation of about 1.5 times the equilibrium values, and diminish very rapidly at larger separations, we may, for large enough cracks (e.g. cracks larger than the smallest microcracks), neglect these forces on the crack faces except at those points near the tip where the atomic bonds are stretched to their maximum. Here the contour of the crack can be considered to close smoothly over a characteristic distance d (figure 2). The condition for the crack to grow, as formulated by Barenblatt,* may now be written approximately as

$$K = \frac{1}{\pi} \int_{c-d}^{c} \frac{F(b)db}{\sqrt{c-b}} \qquad (2.3)$$

with K a stress intensity factor, and $F(b)$ the cohesive forces acting across the crack interface. The smooth closing of the crack removes the stress singularity at the crack contour which appears in the continuum mechanics solutions where cohesive forces are disregarded. However, although d is regarded as small compared with the radius ρ of the crack tip, it is substantially larger than interatomic distances, so that the solutions of continuum mechanics may be applied over distances of order d. It follows that the results of fracture mechanics may be

*The notation used here differs from that used by Barenblatt; it follows instead more conventional fracture mechanics notation. It should also be pointed out that various definitions of "stress intensity factor" appearing in the literature differ by small numerical factors.

used to determine the stress intensity factors $\underline{K}$ in (2.3).

Actually, Barenblatt discussed only cracks extending in their own plane ($\underline{\theta} = 0$) and under only tensile stresses along the crack path ($\underline{K}_\tau = 0$). Putting $\underline{\theta} = 0$, $\underline{K}_\tau = 0$ in (2.2) we interpret Barenblatt's criterion for crack growth by stating that fracture will occur when the crack tip stresses $\underline{T}_o(\underline{r})$ reach a level sufficient to overcome the cohesive forces. Now let us consider the effect of superposing a distribution of shear stresses $\underline{\tau}(\underline{b})$ along the crack path: $\underline{K}_\tau$ is now non-zero and although we do not alter the value of $\underline{T}_o(\underline{r})$ at $\underline{\theta} = 0$ we superpose a shear $\underline{S}_{ro}(\underline{r})$ ahead of the crack tip. Supposing, for the present, the existing crack plane to be one of relative weakness such that the crack can only extend in this plane, we ask whether or not the addition of the shear terms plays any role in the fracture growth. Using the Barenblatt model we need only consider the effects of $\underline{S}_{ro}(\underline{r})$ across the atom layers over the distance $\underline{d}$. To the approximation of isotropic linear elasticity this stress will produce only displacements parallel to the atom layers, and will therefore not work against the surface energy. More detailed calculations (for example, Tyson 1966) show, however, that with shears $\underline{S}_{ro}(\underline{r})$ approaching the theoretical strength of ideal materials, substantial displacements normal to the shear plane may occur, and these displacements will then be free to separate the atom layers along $\underline{d}$ and work against $\underline{\gamma}$. Indeed, we might envisage that a crack could be made to extend in its own plane under the action of pure shears along along the crack path (i.e. $\underline{K}_\sigma = 0$, $\underline{T}_o(\underline{r}) = 0$), the stress level being raised until $\underline{S}_{ro}(\underline{r})$ causes sufficient normal separation across the extension

plane.* With due regard to the complexity of the above situation we may, in noting that shear stresses $\underline{S}_{ro}(\underline{r})$ will be considerably less effective than tensile stresses $\underline{T}_{o}(\underline{r})$ in separating atom layers across $\underline{d}$, conclude that so long as $\underline{S}_{to}(\underline{r}) < \underline{T}_{o}(\underline{r})$ the crack will extend when $\underline{T}_{o}(\underline{r})$ attains a sufficient intensity independent of the superposed $\underline{S}_{ro}(\underline{r})$.

We may now generalize the situation one step further by removing the restriction that the crack must extend in its own plane. To do this we compute the strain energy released by the stresses working against surface energy as the crack extends from some favoured location on the crack tip contour. At the present time solutions for the energy release rate per unit length of crack front $\underline{G}$ are available only for cracks extending in their own plane: we find

$$G_{\sigma} = \frac{\pi}{E} [2r\, T_{o}^{2}]_{r \to o} \qquad (2.4)$$

for plane stress (for plane strain replace $\underline{E}$ (Young's Modulus) by $\underline{E}/(1 - \underline{\nu}^2)$ (ν = Poisson's ratio)), with a similar expression for $\underline{G}_{\tau}$ in terms of $\underline{S}_{ro}$. However, for small deviations from the crack plane

*It might be argued that a crack in pure shear could propagate by a mutual sliding off of layers across the extension plane (termed "sliding mode" in fracture mechanics nomenclature), and that the shear stress necessary to be overcome for this mechanism to operate might be less than that required to be overcome to actually separate atom layers ("opening mode"). However, since the stress field around the crack tip is strongly localized (i.e. falls off as $\underline{r}^{-1/2}$) such a mechanism would, in an otherwise perfect crystal, involve the nucleation and subsequent movement of dislocations or other defects. Since in very brittle materials such mechanisms would provide very large resistance to further propagation of a crack thus formed we will discount such modes and treat our materials as ideally brittle in which surface energy is the only finite term in the resistance to fracture.

(2.4) may be modified to the equation

$$G = \frac{\pi}{E} [2r\ T_\theta^{\,2}]_{r \to o} \qquad (2.5)$$

without much loss in accuracy (Rice, unpublished). (We drop the subscript in (2.5), understanding G to be equivalent to G_σ, for reasons which will be pointed out below.) Balancing the work done by the stresses $T_\theta(r)$ against the surface tension γ, we have

$$G = 2\gamma \qquad (2.6)$$

for an equilibrium crack (Griffith's condition). We then locate the value of θ at the crack tip which first satisfies (2.6), using (2.5) to evaluate the θ-variation of G and taking into account the θ-variation of γ. We thus see that this favoured location is that which maximizes $T_\theta^{\,2}/\gamma$. This may be considered as a modified form of the maximum crack tip tensile stress criterion for isotropic materials, with $T_\theta/\gamma^{\frac{1}{2}}$ replacing T_θ as the quantity to be maximized.

2.2 Calculation of the Crack Path

In the preceding section we proposed a criterion for crack extension, subject to the provisos that the curvature of the crack should not be severe (i.e. θ should be small for each increment of crack extension) and that $S_{r\theta} < T_\theta$ (or, $K_\tau < K_\sigma$). Satisfaction of these provisos for the case of isotropic materials leads to the conclusion already mentioned that crack paths tend to follow stress trajectories. We will now attempt to establish a similar convenient rule for crack paths in single crystals.

We first note the manner in which the stress intensity factors in (2.2) depend on the prior stresses along the crack path. It is seen that the values of $\underline{\sigma}(\underline{b})$ and $\underline{\tau}(\underline{b})$ have rapidly increasing influence as $\underline{b}$ approaches $\underline{c}$. Therefore, to a first approximation, we might consider the $\underline{K}$ terms to be controlled by the prior stresses $\underline{\sigma}(\underline{c})$ and $\underline{\tau}(\underline{c})$ at the position of the existing crack tip. Imposing now the restrictions $\underline{\theta}$ small and $\underline{K}_{\tau} < \underline{K}_{\sigma}$ on (2.1) we have $(2\underline{r})^{1/2}\underline{T}_{\theta} \propto \underline{\sigma}(\underline{c})$ very nearly, so that $\underline{G}$ in (2.5) becomes very nearly proportional to $\underline{\sigma}^2(\underline{c})$. It is now a question of allowing the crack to extend in any number of directions and determining which of these first satisfies (2.6). Thus for isotropic materials the favoured direction will be near to that which maximizes $\underline{\sigma}(\underline{c})$, i.e. which corresponds to a direction of a stress trajectory. The shape of cone cracks in glass (Frank & Lawn 1967, Lawn 1967) may be accurately predicted from this criterion: small deviations between observed and computed crack geometry are readily explained by the fact that the crack tip stresses do in fact depend on the prior stresses along the whole of the crack path, and not only those near the tip, and as a consequence the crack extends as though it possessed a "pseudo-inertia", tending to continue in its existing direction when the relevant stress trajectories have excessive curvature. For anisotropic materials the corresponding favoured direction will then be near to that which maximizes $\underline{\sigma}^2(\underline{c})/\underline{\gamma}$ or $\underline{\sigma}(\underline{c})/\underline{\gamma}^{\frac{1}{2}}$. This is not quite as convenient a criterion as the stress trajectory criterion, since one has to take into account the variation of $\underline{\gamma}$, but with a high speed computer it is not difficult to allow the crack to extend stepwise into a given crystal whose surface energy properties are known.

The fracture criterion (2.6) may be represented by an instructive graphical construction. However, as will be seen in §3 it will be convenient to talk about the quantity $\underline{\gamma}^{-1}$ rather than $\underline{\gamma}$. We therefore first rewrite (2.6) as

$$2G^{-1} = \gamma^{-1} \tag{2.7}$$

for an equilibrium crack. We may represent $\underline{G}^{-1}$ and $\underline{\gamma}^{-1}$ as surfaces in reciprocal energy space. As the loading on the specimen is increased from zero the $\underline{G}^{-1}$ surface contracts from infinity until it intersects the $\underline{\gamma}^{-1}$ surface, and the direction of extension corresponds to the direction of the vector drawn from the origin to the intersecting point (or line, for a plane crack). Let us now write $\underline{\sigma}(\underline{c})$, the prior normal stress on a possible inclined crack increment, in terms of the prior stresses acting on the straight-ahead increment. We have, with $\underline{\sigma}'(\underline{c})$ defined in figure 3,

$$\sigma(c) = \sigma_o(c)\cos^2\theta + \sigma_o'(c)\sin^2\theta - 2\tau_o(c)\cos\theta\sin\theta \tag{2.8}$$

with the subscripts referring to $\underline{\theta} = 0$. With $\underline{G} \propto \underline{\sigma}^2(\underline{c})$ and $\underline{G} = \underline{G}_o$ at $\underline{\theta} = 0$ we have

$$G^{-1} = G_o^{-1}\left[\cos^2\theta + \frac{\sigma_o'(c)}{\sigma_o(c)}\sin^2\theta - 2\frac{\tau_o(c)}{\sigma_o(c)}\cos\theta\sin\theta\right]^{-2} \tag{2.9}$$

very nearly. Figure 3 shows traces of the $\underline{G}^{-1}$ surface for a plane crack, using the crack tip as the origin in reciprocal space and with $\underline{\tau}_o(\underline{c})$ zero.

This diagram indicates how the stress state might influence the stability (direction-wise) of a crack. Suppose our specimen to be isotropic, so that the $\underline{\gamma}^{-1}$ surface is a circle centred on the origin.

If a crack runs into a region in which $\underline{\sigma}_o'(\underline{c})/\underline{\sigma}_o(\underline{c}) > 1$ it will tend to become unstable since the $\underline{G}^{-1}$ surface will intersect the $\underline{\gamma}^{-1}$ surface at a location other than directly ahead of the crack tip. As the ratio $\underline{\sigma}_o'(\underline{c})/\underline{\sigma}_o(\underline{c})$ becomes smaller algebraically the crack is less likely to suffer deviations from its present course since (2.7) is satisfied most readily for straight-ahead extensions. It follows that large compressive stresses applied in the direction of crack propagation act as crack stabilisers, a fact often exploited in cleavage experiments.

We can also see why the crack tends to follow the stress trajectories. If the trajectory corresponding to the principal stress $\underline{\sigma}(\underline{b})$ begins to curve away from a previously planar path the crack, if it proceeds along this previous plane, will enter a region in which $\underline{\tau}_o(\underline{c})$ becomes non-zero. The effect of this shear stress will (for $\underline{\sigma}_o'(\underline{c})/\underline{\sigma}_o(\underline{c}) < 1$) be to deflect the $\underline{G}^{-1}$ curve away from symmetry about the straight-ahead direction, as indicated in figure 4 for the case $\underline{\sigma}_o'(\underline{c})$ zero. The $\underline{G}^{-1}$ surface then intersects the $\underline{\gamma}^{-1}$ circle such that the next increment of crack extension tends to become free of shear; i.e. the shear stress $\underline{\tau}_o(\underline{c})$ acts as a restoring stress when a crack deviates from its trajectory path.

For single crystals the construction is only slightly modified. For the hypothetical material with one plane of weakness described in §2.1 the $\underline{\gamma}^{-1}$ surface would have a finite value at two points on a two-dimensional diagram, and these would always be immediately ahead and behind of an extending crack since the crack could never extend on another plane. In reality the traces of $\underline{\gamma}^{-1}$ surfaces on a given plane in reciprocal energy space would be continuous with maxima and minima. The crack now no longer necessarily extends in the direction of minimum

$\underline{G}^{-1}$, the favoured direction depending very much on the relative sharpness of the minima and maxima of the $\underline{G}^{-1}$ and $\underline{\gamma}^{-1}$ surfaces. For instance, if the crack propagates into a region where $\underline{\sigma}_o'(\underline{c}) \sim \underline{\sigma}_o(\underline{c})$ and $\underline{\tau}_o(c) \sim 0$ we see from figure 2.3 that the maxima in $\underline{\gamma}^{-1}$ will determine the direction of fracture. Under such conditions crystalline materials would tend to fracture only along their easy cleavage planes. In this region the superposition of a shear stress $\underline{\tau}_o(\underline{c})$ will not introduce a pronounced minimum in the $\underline{G}^{-1}$ surface, and will therefore have little effect on the fracture. On the other hand, if $\underline{\sigma}_o'(\underline{c})$ becomes less than $\underline{\sigma}_o(\underline{c})$ algebraically, the minimum in $\underline{G}^{-1}$ becomes increasingly sharper and eventually dominant in determining the fracture direction. Thus the crack will tend more to follow the stress trajectories, as in isotropic materials, and the effect of shear stresses $\underline{\tau}_o(\underline{c})$ will in this case be to maintain the crack path along these trajectories.

3. SURFACE ENERGY REPRESENTATION

We now consider the variation of $\underline{\gamma}$ with crystallographic orientation in crystals having the diamond structure. The surface energy can be calculated as half the work required to break bonds across a separation plane. This procedure is, however, an over-simplification since it does not allow for subsequent relaxation of the surface atoms which undoubtedly occurs. (For instance, see the experimental observations of Lander, Gobeli and Morrison (1963) on fracture surfaces of

silicon and germanium.) Such computations are therefore likely to overestimate γ. From the thermochemical data of Harkins (1942) for diamond and Honig (1957) for silicon and germanium the surface energy of {111} (the set of planes across which a minimum number of bonds are required to be broken to separate the crystal into two pieces) may be readily estimated in the approximate manner outlined above. The values of γ_{111} thus found are shown in table 1, together with values measured by Jaccodine (1963) using a cleavage technique. Ramaseshan (1946) and Jaccodine have listed $\gamma_{hk\ell}$ for several other crystallographic planes using the simple-minded broken bond calculation; table 2 shows their results in which $\gamma_{hk\ell}$ is expressed in units of γ_{111}

A second estimate of the relative variation of γ may be made from observations of crystal growth habit. Diamond is most commonly found in nature in the form of near-perfect octahedra: silicon and germanium also tend, in conditions of equilibrium growth, to assume this form. The faces of the octahedra correspond to {111} planes, thus indicating that these are planes of minimum surface energy. Frank (1963) has demonstrated that the equilibrium crystal shape is the geometrical limiting form of the inverse of the quantity γ^{-1} mapped in reciprocal energy space. The inverse of an octahedron is a cube so that there is a considerable advantage in considering the γ^{-1} surface for diamond structure materials rather than the γ surface, particularly when three-dimensional analysis is required. A vector from the centre of the cube to a corner then represents the reciprocal of the surface energy on planes of the {111} type. Likewise, a vector to the centre of one of the faces corresponds to {100} planes. We can, in fact, readily compute relative values of γ for any crystallographic plane.

As seen in table 2 these values, referred to $\underline{\gamma}_{111}$, compare well with the bond-breaking calculations.

The above evidence is in agreement with the observation that diamond (especially), silicon and germanium show a tendency to cleave on {111} planes. Ramaseshan examined a number of diamond chips and noted that the frequency of occurrence of a given crystallographic plane decreased as its corresponding surface energy fell lower in the order given in table 2. Thus these qualitative observations give confidence in applying the cube $\underline{\gamma}^{-1}$ model to evaluate the variation of reversible fracture surface energy with crystallographic orientation in the diamond structures. They also imply that the elastic anisotropy is not sufficiently great to obscure the main features predicted by the model based on anisotropy in $\underline{\gamma}$ alone.

4. FORMATION OF THE HERTZIAN CRACKS

One of the most striking features of a Hertzian pressure crack in diamond (Howes and Tolansky 1955, Tolansky and Howes 1957, Lawn and Komatsu 1966), germanium (Pugh and Samuels 1963, Johnson 1966) or silicon (figure 5) is the near-polygonal surface trace which reflects the symmetry of the diamond structure. From an analysis of such traces the initial stage of crack propagation near the crystal surface appears to proceed along favourably oriented {111} easy-cleavage planes. However, on examination of the crack below the crystal surface it is always found that the path tends to deviate away from {111} planes toward the Hertzian cone. Figure 6, which shows a cross-sectional view of a pressure crack

made on a (111) surface, illustrates this feature. The plane of figure 6 intersects diametrically opposite sides of the near-hexagonal trace in figure 5: {111} planes inclined at 70.5° to the crystal surface extend downward and inward from the left hand side of the trace and downward and outward from the right hand side. Both sides of the internal crack however, spread downward and outward, and away from the {111} planes in a non-symmetrical manner due to the asymmetry of the {111} planes with respect to the (111) crystal surface. In a similar manner the internal crack deviates outward from the {111} planes extending perpendicularly into the crystal from four sides of the (irregular) hexagonal surface trace on the (110) surface (figure 5). Thus there appears to be a conflict between the tendency for the crack to continue to propagate along cleavage planes and for it to follow stress trajectories of the two lesser of the three principal stresses as in isotropic materials.

We now consider the elastic stress situation in the flat specimen beneath the spherical indenter prior to fracture occurring. Using the same notation as used in the paper by Frank & Lawn (1967) the radius $\underline{a}$ of the area of contact between indenter and specimen is given by

$$a^3 = \frac{4}{3}\frac{k}{E} P r \qquad (4.1)$$

where $\underline{k} = (9/16)[(1 - \underline{\nu}^2) + (\underline{E}/\underline{E}')(1 - \underline{\nu}'^2)]$; the primes refer to the indenter material. The greatest tensile stress in the system occurs at the circle of contact, and is radially directed in the crystal surface; its magnitude is

$$\sigma_m = \frac{1-2\nu}{2} p_o \,, \qquad (4.2)$$

where

$$p_o = \frac{P}{\pi a^2} \tag{4.3}$$

is the mean pressure between sphere and specimen. The general stress field in an isotropic specimen is given by the equations of Huber (1904) and Hamilton & Goodman (1966).

In examining the growth of a Hertzian fracture in glass it was concluded that in most instances the crack initiates at or very close to the circle of contact and runs around this circle, but with a somewhat exaggerated radius of curvature because of the "pseudo-inertia" mentioned in §2, producing first a shallow surface ring crack eccentric relative to the circle of contact. The hypothesis that the surface ring forms before subsequent downward extension into the material was based on the knowledge that the prior stresses acting across the ultimate crack surface barely decrease from the value $\underline{\sigma}_m$ at the starting point as one follows the surface trace and that, in marked contrast, they drop off extremely rapidly (to $\underline{\sigma}_m/16$ in a distance of $\underline{a}/50$) along the downward crack path. Although in the present case of interest the surface traces deviate further from the circle of contact than their counterparts in glass the weight of the above argument is barely lessened; one may therefore infer that the crack initiates at one point and runs around both sides in an unstable manner to complete itself on the opposite side. (This conclusion has some experimental support (Howes & Tolansky 1955).) One may then consider the downward propagation of the surface crack.

This model of crack formation permits one to reduce the problem of Hertzian crack formation to two plane problems. Firstly, in considering

the surface crack we need only consider the stressfield at or very near to the surface of the specimen, since these stresses are shallow. In the limit of an infinitely shallow surface ring we have conditions of plane stress operating: in view of the argument presented in the previous paragraph this approximation would appear to be satisfactory. Secondly, with regard to the subsequent downward extension of the crack we may, so long as $\underline{c}$ is not comparable with $\underline{a}$, consider the crack to be propagating under conditions of plane strain. Certain complicating features in this second stage of crack growth may arise to lessen the effectiveness of the plane strain approximation; these will be discussed briefly in §4.2.

With plane stress or plane strain operative the application of the graphical construction outlined §2.2 for determining crack paths becomes straightforward. For plane stress the $\underline{G}^{-1}$ surface is a right prism with axis parallel to the crack edge. We need only in this case consider the <u>projection</u> of the $\underline{G}^{-1}$ and $\underline{\gamma}^{-1}$ surfaces on to the plane normal to the crack edge: for the diamond structure materials the projection of the $\underline{\gamma}^{-1}$ cube will be polygonal in shape. The plane strain case is slightly more complicated. Here the shape of the $\underline{G}^{-1}$ surface will depend on the relative magnitude of the principal stress acting out of the plane normal to the crack edge (hereafter referred to as the "normal plane"). If this normal stress is compressive, as it is for the case of the downward propagating crack, the $\underline{G}^{-1}$ surface possesses a convexity (with respect to the origin at the crack tip) in the plane of the crack itself. (This fact can be derived from figure 3.) We assume that this convexity is sufficient that the $\underline{G}^{-1}$ and $\underline{\gamma}^{-1}$ surfaces intersect on the normal plane containing the origin

in reciprocal space. With this assumption we need only consider the trace of the $\underline{G}^{-1}$ and $\underline{\gamma}^{-1}$ surfaces on the above normal plane.

We now consider the two stages of crack formation in turn. For simplicity the effects of "pseudo-inertia" will be neglected: its presence will lead only to a slight eccentricity of the computed crack geometry with respect to the axis perpendicular to the centre of contact.

4.1 The Surface Crack

It was argued above that the surface crack forms under plane stress conditions, for which we will have to consider the projections of the $\underline{\gamma}^{-1}$ surface on to the plane of the crystal specimen surface. For three common surface orientations this projection is shown in figure 7. The crack is shown progressing in a favored direction (below). Its tip is at the centre of reciprocal energy space.

The procedure for calculating the path of the surface crack begins with a sub-microscopic flaw located at the circle of contact, where the tensile stresses are greatest. The most favorable location on this circle of contact is then chosen as the likely starting point for the crack. This location may be deduced from figure 7 as that whose tangent to the circle of contact corresponds in direction with that of the maximum reciprocal lattice vector. The crack is then allowed to extend stepwise, each increment of extension following the direction of maximum $\underline{\sigma}_o(\underline{c})/\underline{\gamma}^{\frac{1}{2}}$ computed at the location of the crack tip, until the crack has extended around to the opposite side of the circle of contact. (By the symmetry of the problem the crack is taken to extend simultaneously

around both sides of the circle.) The effects of curvature of the crack are minimised by taking sufficiently small increments of crack growth.

The graphical construction in §2.2 is useful for providing visual insight into probable crack behaviour. The surface crack propagates in a region of free surface outside the circle of contact where the two principal stresses are always equal and opposite. Thus $\underline{\sigma}_o'(\underline{c})$ is compressive, and is equal to $-\underline{\sigma}_o(\underline{c})$ always, so that the $\underline{G}^{-1}$ surface is convex, as in figure 3. Thus by mere inspection of the nature of the $\underline{G}^{-1}$ and $\underline{\gamma}^{-1}$ surfaces it may be seen that the vertices of the latter will correspond to favoured but not dominant directions of crack growth. As the crack propagates from the circle of contact along a favoured direction and thus deviates from the stress trajectory (in this case coincident with the circle of contact) it experiences an increasing shear stress $\underline{\tau}_o(\underline{c})$ which tends to restore the crack back toward the circle. The computed crack paths (figure 8) are consistent with this description; they show a compromise between propagation in the directions corresponding to the $\underline{\gamma}^{-1}$ vertices and propagation around the circle of contact. These traces compare favourably with those illustrated in figure 5.

4.2 The Downward-extending Crack

Since the tensile stresses attain their maximum at the circle of contact it seems reasonable to presume that the downward-extension of the crack begins near there. Consequently we will consider cross-sections of the crystal passing through the axis of symmetry and through the favoured starting points of the surface crack. Since plane strain

is assumed to apply to such cross-sectional planes we consider their intersection with the $\underline{\gamma}^{-1}$ surface (figure 9). The direction of initial extension downward may be evaluated by noting that at the circle of contact $\underline{\sigma}'_o(\underline{c})$ is zero. Thus the crack begins in a region of uniaxial tension which, according to figure 3, corresponds to a quite convex $\underline{G}^{-1}$ surface whose minimum is located perpendicularly beneath the circle of contact.

The procedure for computing the crack paths is carried out as for the surface crack. However, in the case of the downward-extending crack it is found that the crack rapidly moves from the region of $\underline{\sigma}'_o(\underline{c}) = 0$ to a region where $\underline{\sigma}'_o(\underline{c}) \sim -10\underline{\sigma}_o(\underline{c})$, and it experiences a stress state of the second type for most of its journey within the crystal. We see from figure 3 that this corresponds to a very pointed $\underline{G}^{-1}$ surface, so that the crack path is very much dictated by the stress trajectory pattern and not so much by the maxima and minima in the $\underline{\gamma}^{-1}$ surface. This explains the experimental observation that the downward crack profile tends to resemble that of the conventional cone crack in glass. Because all Hertzian cracks in the diamond structure crystals assume much the same form well below the surface the entire computed crack paths are not included in figure 10; only the more interesting region down to a very small distance below the surface, where the transition between the two stress regimes occurs, is illustrated. (For comparison purposes traces of the stress trajectory surface and of {111} planes are included.) It is difficult to compare the computations in figure 10 with experiment because of the small distances characterising the transition region, but the prediction that for the (111) surface orientation the internal cracks begin on the inclined {111} planes, and

as the energy release rate for a surface crack in a semi-infinite medium. Although our downward extending cracks are curved the form of (5.1) will not be in error, only the numerical constants will suffer from inaccuracy. We now make use of the geometrical similarity of the Hertz elastic problem by expressing stresses in terms of p_o and lengths in terms of a. Thus we will find it convenient to re-define K_σ in (2.2) in terms of the dimensionless quantity

$$K = \frac{2.24}{\pi}\left(\frac{c}{a}\right)^{\frac{1}{2}} \int_o^{c/a} \frac{\sigma/p_o \; d(b/a)}{(c^2/a^2 - b^2/a^2)^{1/2}} \tag{5.2}$$

so that we have $K_\sigma = p_o a^{\frac{1}{2}} K$, which yields

$$G = \frac{\pi}{E}(1 - \nu^2) p_o^2 \, a \, K^2 \quad . \tag{5.3}$$

Eliminating p_o and a from (5.3) using (4.3) and (4.1) we have

$$G = \frac{3P(1 - \nu^2)}{4\pi kr} K^2 \quad . \tag{5.4}$$

In writing $G > 2\gamma$ as the condition that a crack should extend we must take note of the fact that a curved crack will, during the course of its growth, experience a wide range of γ. We will subsequently find it advantageous to write $\gamma = \gamma_{111}(\gamma/\gamma_{111})$ so that for an equilibrium crack

$$\frac{3P(1 - \nu^2)}{4\pi kr} K^2 = 2\gamma_{111}\left(\frac{\gamma}{\gamma_{111}}\right) \quad . \tag{5.5}$$

The quantities K^2 and γ/γ_{111} may be determined numerically at any point along the crack path. Collecting these into one term

$$\Phi = \frac{1}{K^2} \frac{\gamma}{\gamma_{111}} \tag{5.6}$$

rapidly (particularly the crack on the left hand side in figure 10) depart from these planes just below the surface, is in accord with the example shown in figure 6.

So far we have assumed that the internal cracks extend downward in a perfectly smooth manner. However, the observation of fracture irregularities at the internal fracture interfaces in diamond by Howes & Tolansky indicate that there is mutual interference from the extensions from adjacent sides of the surface traces. Presumably there is difficulty in accommodating any relative shape change of different sections of the crack as it penetrates into regions of different stress state. This effect may be envisaged by considering the crack profile for the (111) surface orientation. Alternate sides of the hexagonal surface trace will extend downward along geometrically different paths as shown in figure 6: this will necessarily give rise to conflict in the regions common to the alternate sides. However, as will be seen in the next section, the mechanics of the downward extending crack are critically determined by its behaviour down to a depth of about 0.1 $\underline{a}$, where such secondary effects should have little influence.

5. MECHANICS OF FRACTURE

5.1 Theoretical

From (2.1) and (2.5) we may write, for $\underline{\theta}$ small and $\underline{K}_\tau < \underline{K}_\sigma$, and for conditions of plane strain,

$$G = \frac{\pi}{E}(1 - \nu^2)K_\sigma^2 \qquad (5.1)$$

and writing

$$H = \frac{3(1 - \nu^2)}{8\pi k \gamma_{111}} \frac{P}{r} \tag{5.7}$$

we arrive at the following as the condition that a crack should extend:

$$\Phi < H \ . \tag{5.8}$$

It is to be noted that Φ depends only on the geometry of the cracks for a crystal of given surface orientation. Figure 11 shows Φ as a function of relative length along the downward crack paths partially illustrated in figure 10, together with the isotropic case for comparison. (In the case of the (111) surface orientation only the crack shown on the right hand side of figure 10 is represented in figure 11 since its value of Φ^* is the smaller and, as will be seen below, it is this parameter which determines the critical loading condition.) The quantity H, on the other hand, is independent of crack length and is thus representable in figure 11 as a horizontal line whose height is proportional to the load exerted by the indenter on the specimen. A crack of given length is then in equilibrium when the H line is raised to intersect the value of Φ appropriate to this length. Different branches of the Φ curves, distinguished by the labels c_o, c_1, c_2, and c_3 in figure 11, then represent different types of crack equilibrium. These branches have been discussed in detail previously by Frank & Lawn (1967) (for a more general discussion of crack stability in the equilibrium sense reference in again made to the paper by Barenblatt (1962)). It is sufficient to say here that the equilibrium is stable or unstable according to whether or not $d\Phi/dc$ is positive or negative.

The appearance of the maximum in each of the curves in figure 11 is the main feature of interest since it is this which is responsible for the existence of Auerbach's law. In §4 we assumed the initial stage of crack growth to begin from a sub-microscopic flaw at the circle of contact. Writing the depth of this crack in the downward-extending direction as $\underline{c}_f$ we represent the flaw by a point $(\underline{c}_f/\underline{a}\ ,\ \underline{H})$ in figure 11. At zero load this point is located at infinity on the $\underline{c}/\underline{a}$ axis (since $\underline{c}_f/\underline{a}$ is proportional to $\underline{P}^{-1/3}$): as the load on the indenter is applied the point migrates along a curve of the form $(\underline{c}_f/\underline{a})^3\underline{H}$ = constant ($\underline{H}$ being proportional to $\underline{P}$) in the direction of the arrows in figure 11 until it intersects the $\underline{\Phi}$ curve. We consider this intersection to occur somewhere between $\underline{c}_o^*$ and $\underline{c}^*$. If it occurs on the $\underline{c}_o$ branch an incremental increase in load will cause the crack to proceed unstably toward the $\underline{c}_1$ branch at constant load (i.e. along the $\underline{H}$ line). When the stable $\underline{c}_1$ branch is reached (or if intersection first occurs there) further gradual increases in load will be required to raise $\underline{H}$ and thus permit the crack to grow along the $\underline{\Phi}$ curve in a stable manner until $\underline{c} > \underline{c}^*$ (or, $\underline{H} > \underline{\Phi}^*$). This final stage in which the crack is "pushed over the hill" to proceed at constant load to $\underline{c}_3$ represents the development of the visible Hertzian crack. From (5.8) and (5.7) and figure 11 we see that the condition for this to happen may be written

$$\frac{\underline{P}^*}{\underline{r}} > \frac{8\pi k\gamma_{111}\Phi^*}{3(1-\nu^2)} \sim 4 \times 10^5 k\gamma_{111} \qquad (5.9)$$

This establishes Auerbach's law $\underline{P}^*/\underline{r}$ = constant and specifies that the Auerbach constant is proportional to $\underline{\gamma}_{111}$.

5.2 Experimental

Some indentation tests were performed on silicon with a view to investigating the Auerbach law. All specimens tested were cut from one single crystal of "Lopex" grade silicon (n-type, specific resistivity 1.5 ohm cm^{-1}, dislocation density $< 500\ cm^{-2}$) purchased from Texas Instruments. The specimens, at least 2 cm thick, were shaped with major surface orientations within 1° of (100), (111) or (110) planes. The tests were carried out on an Instron testing machine, using sintered tungsten carbide Brinell balls as indenters; the crosshead was driven at a speed of 0.005 cm sec^{-1} in all experiments described in this section. Because of the difficulty in determining the precise instant of fracture in the opaque silicon a systematic series of indentations, with maximum load as variable, was made on each specimen with five balls. The specimens were then etched in a solution of 90% HNO_3 + 10% HF, thereby revealing which indentations had produced fully developed Hertzian fractures. The critical load $\underline{P}_c$ could, under favourable conditions of specimen preparation (see below), be determined to within about ±5%, an uncertainty which accounts for nearly all the scatter in the results presented below.

The first experiments were made on specimens prepared carefully by using 0.3 μm alumina powder as a final mechanical polish and by following with a light chemical polish. The measured critical load for a given indenter on these specimens showed a scatter of up to 100%. This was attributed to a lack of sizeable flaws in the range $\underline{c}_o^* \leq \underline{c}_f \leq \underline{c}^*$, the condition necessary for Auerbach's law to be established. The specimen surfaces were then abraded with No. 600 SiC paper: according

to Stickler & Booker (1963) such treatment introduces an abundance of surface cracks down to a depth of about 10 μm. From figure 11 the condition for Auerbach's law to be established now becomes approximately $5 \times 10^{-3}\ \underline{a} \leqslant 10^{-3}\text{cm} \leqslant 10^{-1}\ \underline{a}$. Eliminating $\underline{P}$ from (4.1) and (5.9) and substituting the resulting expression for $\underline{a}$ into this condition we arrive at upper and lower limits of indenter radius within which Auerbach's law might be expected to hold: inserting $\underline{\gamma}_{111} \sim 1.4 \times 10^{3}$ ergs cm^{-2} and $\underline{E} \sim 1.3 \times 10^{12}$ dynes cm^{-2} for silicon and $\underline{k} \sim 0.8$ for tungsten carbide indenter on silicon we thus have $5 \times 10^{-2}\ \text{cm} \leqslant \underline{r} \leqslant 5\ \text{cm}$ approximately. This embraces the range of indenter size used in these experiments. The abrading procedure, apart from increasing the flaw <u>size</u>, also increases the flaw <u>density</u>, thereby improving the liklihood of initiating the Hertzian crack at the most favourable location on the circle of contact, as was assumed in §4. The results obtained with specimens prepared in this way are shown in figure 12 in which $\underline{P}_c/\underline{r}$ is plotted as a function of $\underline{r}$. Within the experimental scatter it is seen that Auerbach's law is indeed satisfied for the three surface orientations, so that we may identify $\underline{P}_c$ with $\underline{P}^*$. (The full lines drawn through the points represent mean values of $\underline{P}^*/\underline{r}$.) It is noted that $\underline{P}^*/\underline{r}$ increases in the order (111) , (110) , (100) ; this does not correlate exactly with the order (111) , (100) , (110) predicted by figure 11, but in view of the numerical uncertainty in the theoretical treatment and the experimental scatter this is not surprising.

Another experiment was performed in order to test the effect of varying the flaw size $\underline{c}_f$. From figure 11 it is seen that flaw size should have no effect on $\underline{P}^*/\underline{r}$ so long it falls within the limits $\underline{c}_o^*$ and $\underline{c}^*$. Indentations made on specimens abraded with No. 320 SiC paper

(which, according to Stickler & Booker, would introduce surface cracks down to about 20 μm) showed no systematic deviation from the results in figure 12. This therefore confirms that the Auerbach constant is independent of the flaw size, so that no stringent surface preparation of samples, other than ensuring that an adequate amount of flaws are present, is necessary in the Hertzian fracture test.

6. DISCUSSION

The geometry and mechanics of Hertzian cracks in diamond structure materials have been computed on the assumption that the anisotropy in surface energy dominates over that in the elastic constants. All essential features of the observed crack behaviour are accounted for by the computations, although the effects of crystallographic fracture appear to be slightly under-estimated, especially in diamond where the surface traces are more strictly polygonal than indicated in figure 8. A more formal treatment of the problem, for instance by applying the fracture mechanics analysis of Sih, Paris & Irwin (1965) to the Hertzian stress field in an anisotropic material (Willis 1966), might be expected to give more exact correspondence between theory and observation. However, these two above papers reveal that even for cubic crystals the mathematics involved would be formidable, and in view of the fact that other approximations (e.g. neglecting effects of crack curvature, considering the crack to grow under plane conditions, etc.) contribute to the uncertainty in the treatment the more refined calculations are not considered warranted here.

The theoretical prediction that Auerbach's law should hold for diamond structure crystals has been confirmed in experiments on three major surface orientations of silicon. Therefore, because the approach to the Auerbach condition $\underline{\phi}^* = \underline{H}$ is one of stable crack growth along $\underline{c}_1$, measurement of the Auerbach constant $\underline{P}^*/\underline{r}$ in (5.9) affords a convenient means for determining the reversible fracture surface energy $\underline{\gamma}$. However, due to the approximations made in the theoretical treatment any such determination of the absolute value of $\underline{\gamma}$ will be unreliable, but relative values may, in principle, be measured with the same degree of accuracy as the Auerbach constant. This raises the possibility of using the Hertzian test to investigate certain mechanical properties of brittle crystals. For instance the strength of a given material may be readily measured as a function of temperature (providing no significant change in elastic anisotropy occurs), environmental atmosphere, irradiation dosage, impurity content, loading conditions etc. And the Hertzian fracture test has the advantage that the Auerbach condition is independent of flaw statistics, so that small specimens requiring no stringent preparation other than ensuring a reasonably flat, flaw-abundant surface may be used. Some preliminary experiments aimed at investigating the fatigue properties of brittle crystals indeed indicate that the strength of silicon is dependent on the number of loading cycles.

Having stated that $\underline{\gamma}$ should be accurately measureable in a relative sense it is tempting to take values of the Auerbach constant for diamond, silicon and germanium and observe how well they compare with the $\underline{\gamma}$ values listed in table 1. Unfortunately data is not available for germanium but Howes (1959, 1962) has accumulated results

of scattered tests on diamond. Only for the (111) surface of diamond are there sufficient data to indicate that Auerbach's law holds within limits of experimental scatter. In table 3 mean values of $\underline{P}^*/\underline{kr}$ from Howes' data are compared with values for silicon. It is seen that diamond is characterised by a considerably wider variation in values of the Auerbach constant for the three surface orientations than would be expected from figure 11. (It has already been pointed out that diamond also deviates the most from theoretical expectation insofar as crack geometry is concerned.) We may, however, conclude that the generally larger values of $\underline{P}^*/\underline{kr}$ for diamond are commensurate with the larger value of $\underline{\gamma}$ for this material as compared with silicon.

ACKNOWLEDGEMENTS

The author wishes to express his gratitude to Professor F. C. Frank, University of Bristol, for many discussions and for his interest in this work. Dr. Stephen Burns and Professor James Rice also contributed useful discussion regarding the crack extension criterion outlined in §2. Part of this work was financed by Industrial Distributors and the remainder by an ARPA contract.

REFERENCES

AUERBACH, F. 1891 Ann. Phys. Chem. 43, 61.

BARENBLATT, G.I. 1962 Adv. Appl. Mech. 7, 55.

ERDOGAN, F. & SIH, G.C. 1963 J. Basic Engin. 85, 519.

FRANK, F.C. 1963 Metal Surfaces: Structure, Energetics and Kinetics. (A.S.M. publication), Ch. 1.

FRANK, F.C. & LAWN, B.R. 1967 Proc. Roy. Soc.

GRIFFITH, A.A. 1920 Phil. Trans. A 221, 163.

GRIFFITH, A.A. 1924 First Internat. Congr. Appl. Mech. (Delft), 55.

HAMILTON, G.M. & GOODMAN, L.E. 1966 J. Appl. Mech 33, 371.

HARKINS, W.D. 1942 J. Chem. Phys. 10, 268.

HONIG, R. 1957 R.C.A. Rev. 18, 203.

HOWES, V.R. 1959 Proc. Phys. Soc. 74, 48.

HOWES, V.R. 1962 Proc. Phys. Soc. 80, 78.

HOWES, V.R. 1965 Physical Properties of Diamond. Ed. Berman. (Oxford: Clarendon Press), Chap. VI.

HOWES, V.R. & TOLANSKY, S. 1955 Proc. Roy. Soc. A 230, 287, 294.

HUBER, M.T. 1904 Ann. der Physik. 14, 153.

HUNTINGTON, H.B. 1958 Solid State Phys. 7, 213.

JACCODINE, R.J. 1963 J. Electrochem. Soc. 110, 524.

JOHNSON, O.W. 1966 J. Appl. Phys. 37, 2521.

LANDER, J.J., GOBELI, G.W. & MORRISON, J. 1963 J. Appl. Phys. 34, 2298.

LAWN, B.R. 1967 Proc. Roy. Soc.

LAWN, B.R. & KOMATSU, H. 1966 Phil. Mag. 14, 689.

PUGH, E.N. & SAMUELS, L.E. 1963 Phil. Mag. 8, 301.

RAMASESHAN, S. 1946 Proc. Indian Acad. Sci. A 24, 114.

SIH, G.C., PARIS, P.C. & IRWIN, G.R. 1965 Internat. J. Fract. Mech. 1, 189.

STICKLER, R. & BOOKER, G.R. 1963 Phil. Mag. 8, 859.

TOLANSKY, S. & HOWES, V.R. 1957 Proc. Phys. Soc. B 70, 521.

TYSON, W.R. 1966 Phil. Mag. 14, 925.

WILLIAMS, M.L. 1957 J. Appl. Mech. 24, 111.

WILLIS, J.R. 1966 J. Mech. Phys. Solids 14, 163.

TABLE 1

Surface energy for {111} plane (ergs cm^{-2})

	Calculated	Measured
Di	5700	
Si	1410	1230
Ge	1150	1060

TABLE 2

Values of $\gamma_{hk\ell}/\gamma_{111}$ for some crystallographic planes in crystals with the diamond structure

Plane	Calculation (bonds broken)	Model (γ^{-1}cube)
111	1.000	1.000
221	1.154	1.155
110	1.225	1.225
211	1.415	1.414
210	1.550	1.549
100	1.732	1.732

TABLE 3

P^*/kr (kg cm^{-1}) for diamond (Howes 1959, 1962) and silicon

	(100)	(111)	(110)
Di	617	90	175
Si	68	54	60

FIGURE CAPTIONS

1. Local tensile stress $\underline{T}_\theta$ and shear stress $\underline{S}_{r\theta}$ acting on incremental area of plane crack.

2. Schematic representation of equilibrium crack tip contour. (See text.)

3. Forms of the $\underline{G}^{-1}$ surface for plane crack. (a) shows stress state at ultimate location of crack tip prior to fracture occurring. $\underline{\tau}_o(\underline{c})$ is zero. (b) shows traces of $\underline{G}^{-1}$ surface. Subscripts are dropped here for convenience. Scale is such that $\underline{G}^{-1} = \underline{G}_o^{-1}$ for $\underline{\theta} = 0$.

4. Forms of the $\underline{G}^{-1}$ surface for plane crack. (a) shows prior stress state at crack tip. $\underline{\sigma}_o'(\underline{c})$ is zero. (b) shows traces of $\underline{G}^{-1}$ surface.

5. Traces of Hertzian cracks on (100), (111), (110) surfaces of silicon. Specimens abraded, indented, etched and viewed in normally reflected light. (Some abrasion scratches are still visible.) $\underline{r}$ = 0.64 cm, $\underline{a}$ = 0.05 cm. Incompleted traces are due to specimen surface not being perfectly normal to line of application of load.

6. Cross-sectional profile of Hertzian crack made on (111) surface of silicon. Direction normally outward from plane of diagram is $[01\bar{1}]$. Specimen sawn through crack, abraded, lightly etched and viewed in obliquely reflected light. $\underline{r}$ = 1.27 cm, $\underline{a}$ = 0.07 cm.

7. Projection of $\underline{\gamma}^{-1}$ cube on to plane of (100), (111), (110) crystal surfaces. The crack orientations shown indicate favoured directions of crack initiation on the circle of contact.

8. Calculated traces of Hertzian cracks on (100), (111), (110) surfaces. The traces circumscribe the circle of contact since no allowance is made for the pseudo-inertia of the crack.

9. Trace of $\underline{\gamma}^{-1}$ cube on to cross-sectional planes (011), $(01\bar{1})$, $(\bar{1}12)$ corresponding to (100), (111), (110) crystal surface orientations respectively. Broken lines indicate traces of the crystal surfaces. The crack orientation shown indicates initial direction of downward extension of crack. (Extension in direction of vertices corresponds to fracture on {111} planes.)

10. Downward extension of cracks (full lines) from (100), (111), (110) surface orientations. Planes of diagram as for figure 9. Extension to depth 0.005 $\underline{a}$ below surface shown. Light lines are traces of stress trajectory surface, broken lines are traces of {111} planes. (The right hand side crack trace for the (111) surface orientation coincides with the {111} plane trace down to the depth shown.)

11. Parameter $\underline{\Phi}$ as a function of relative crack length $\underline{c}/\underline{a}$ for (100), (111), (110) surface orientations, with isotropic case included for comparison. Computed on basis of $\underline{\nu} = 1/3$.

12. $\underline{P}^{*}/\underline{r}$ as function of $\underline{r}$ for (100), (111), (110) surface orientations of silicon.

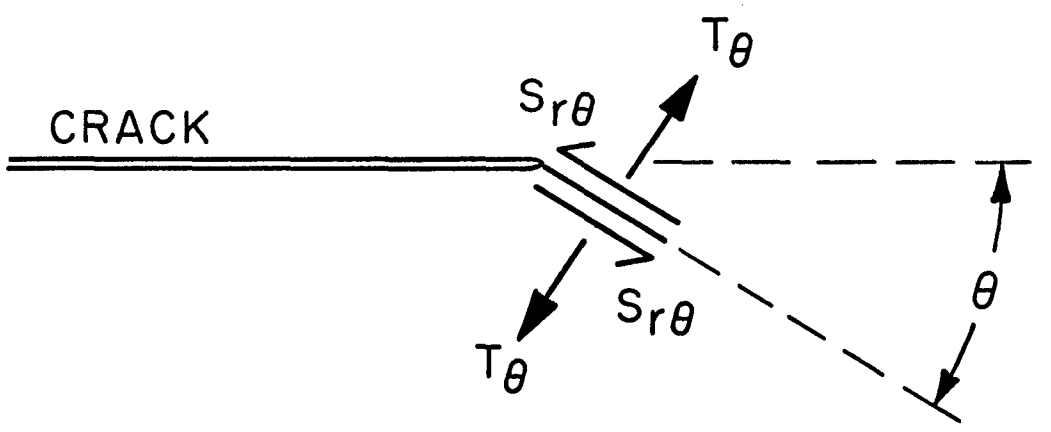

FIGURE 1

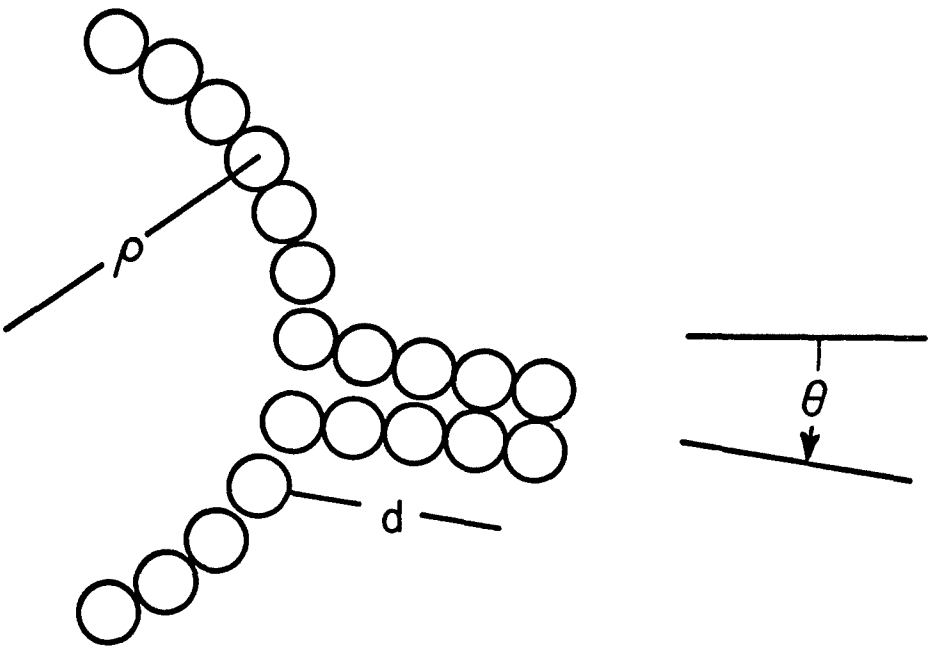

FIGURE 2

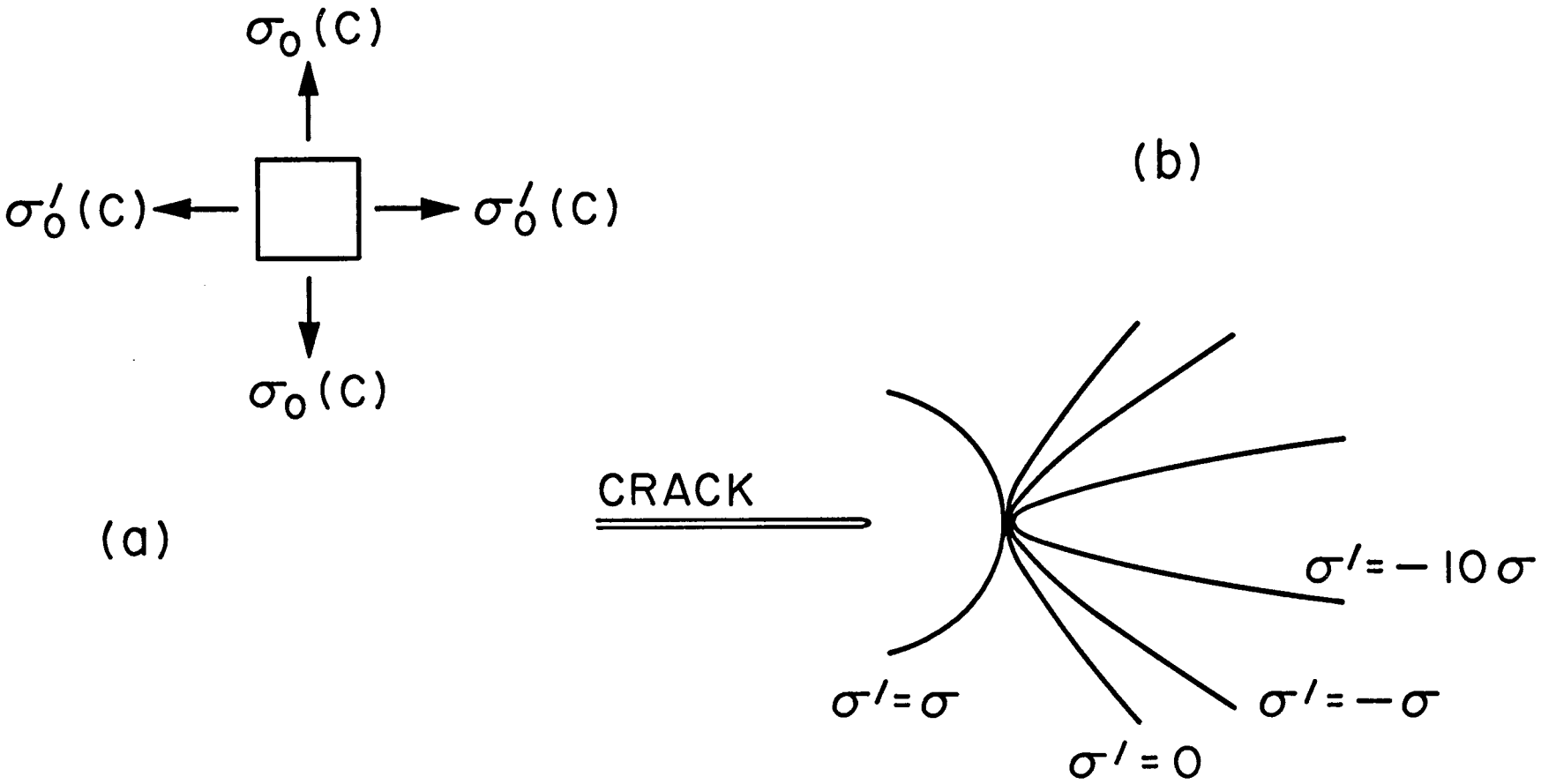
$\sigma_0(C)$
$\sigma_0'(C)$
$\sigma_0'(C)$
$\sigma_0(C)$
(a)
(b)
CRACK
$\sigma' = -10\sigma$
$\sigma' = \sigma$
$\sigma' = -\sigma$
$\sigma' = 0$

FIGURE 3

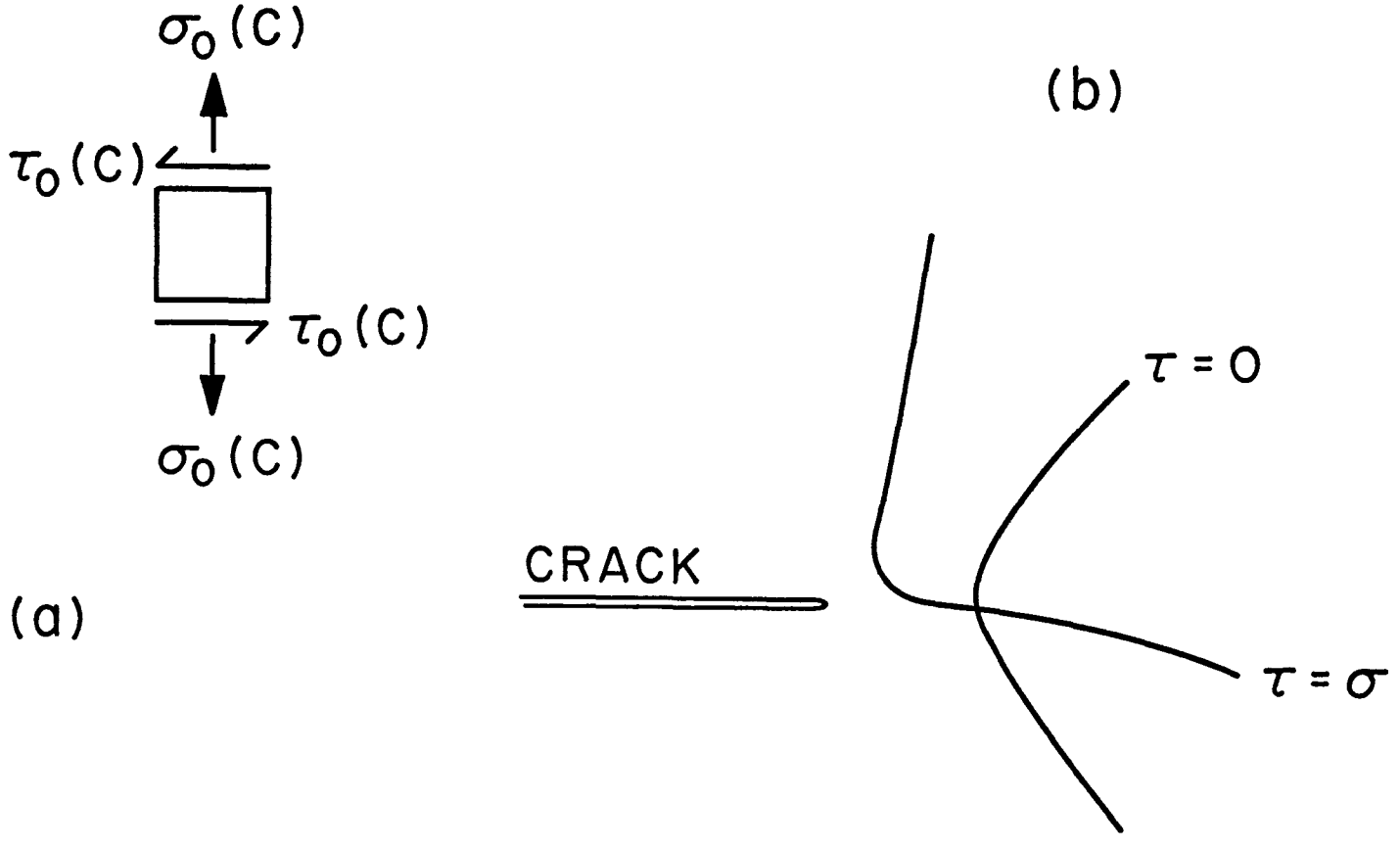

FIGURE 4

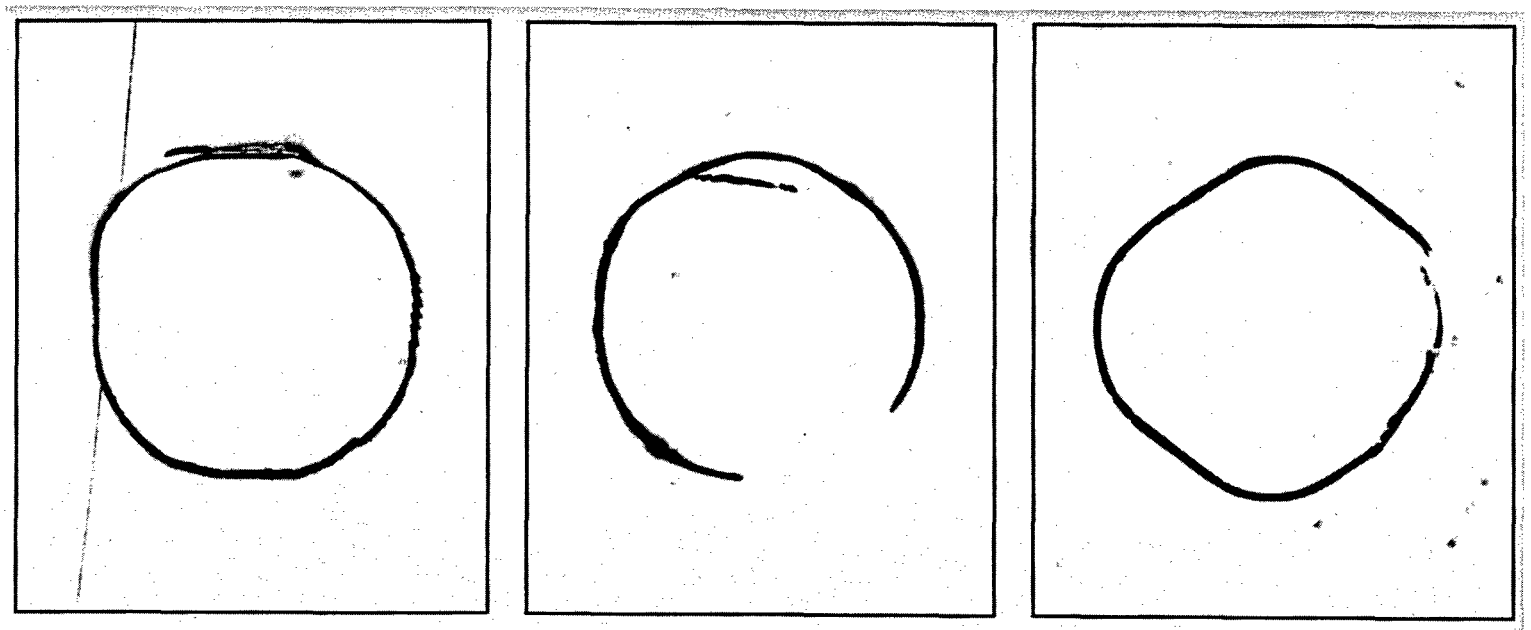

(100) (111) (110)

FIGURE 5

FIGURE 6

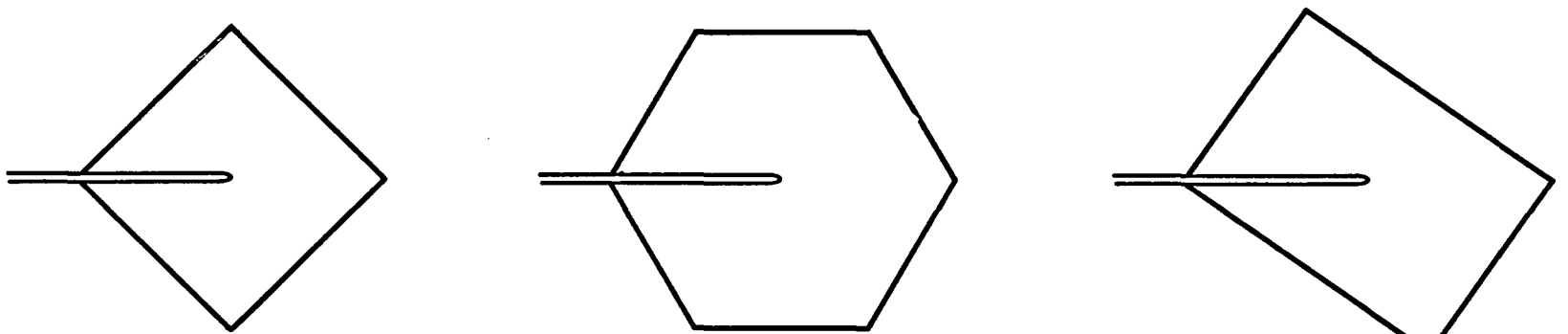

FIGURE 7

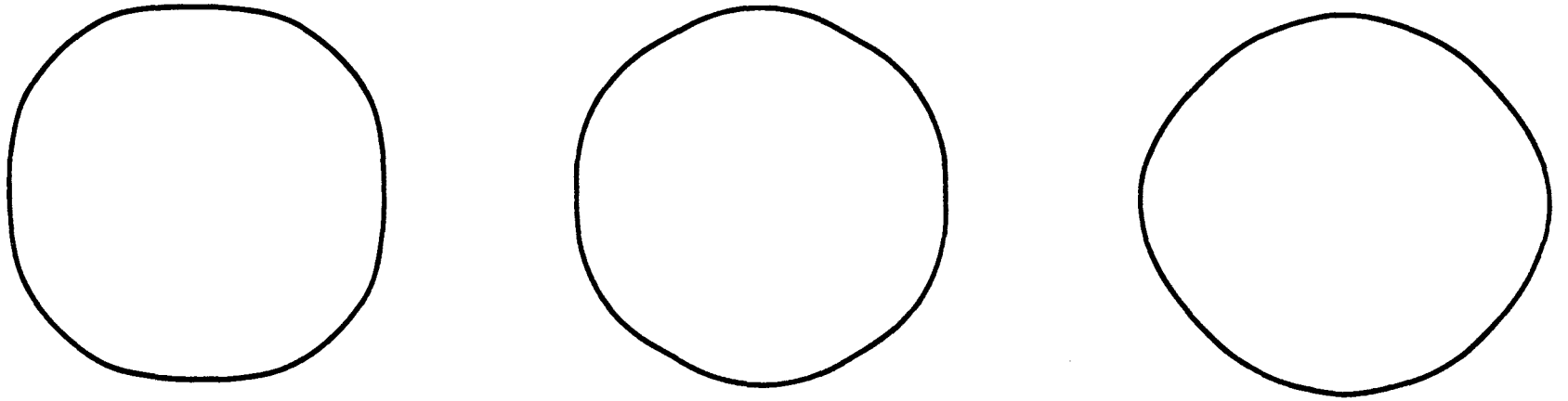

FIGURE 8

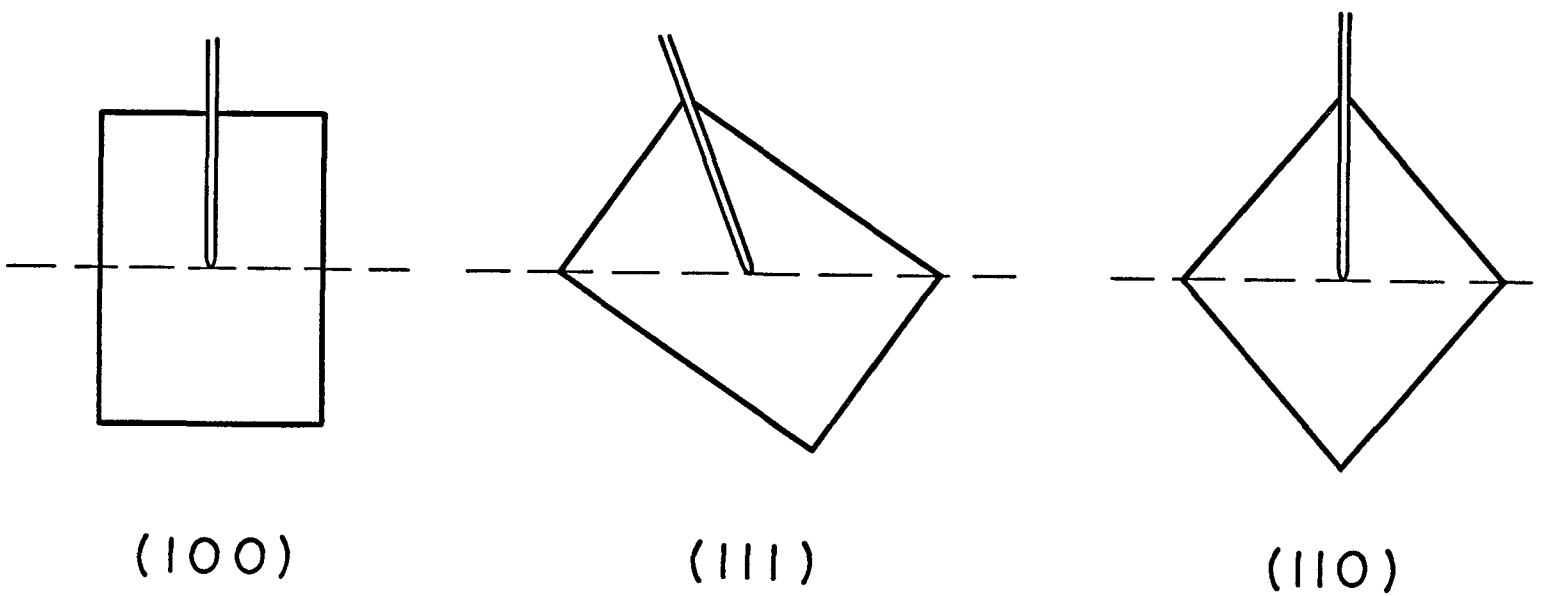

FIGURE 9

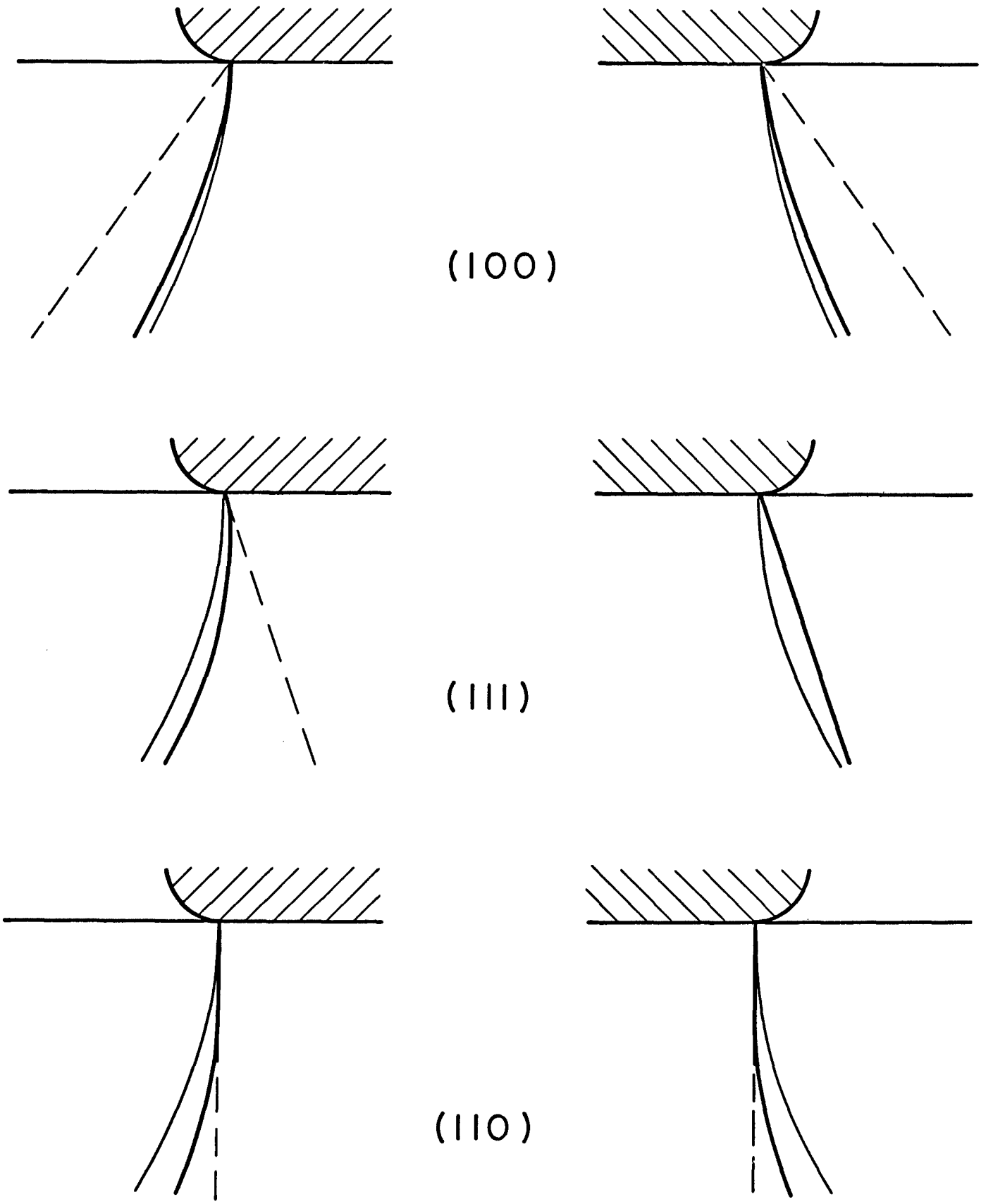

FIGURE 10

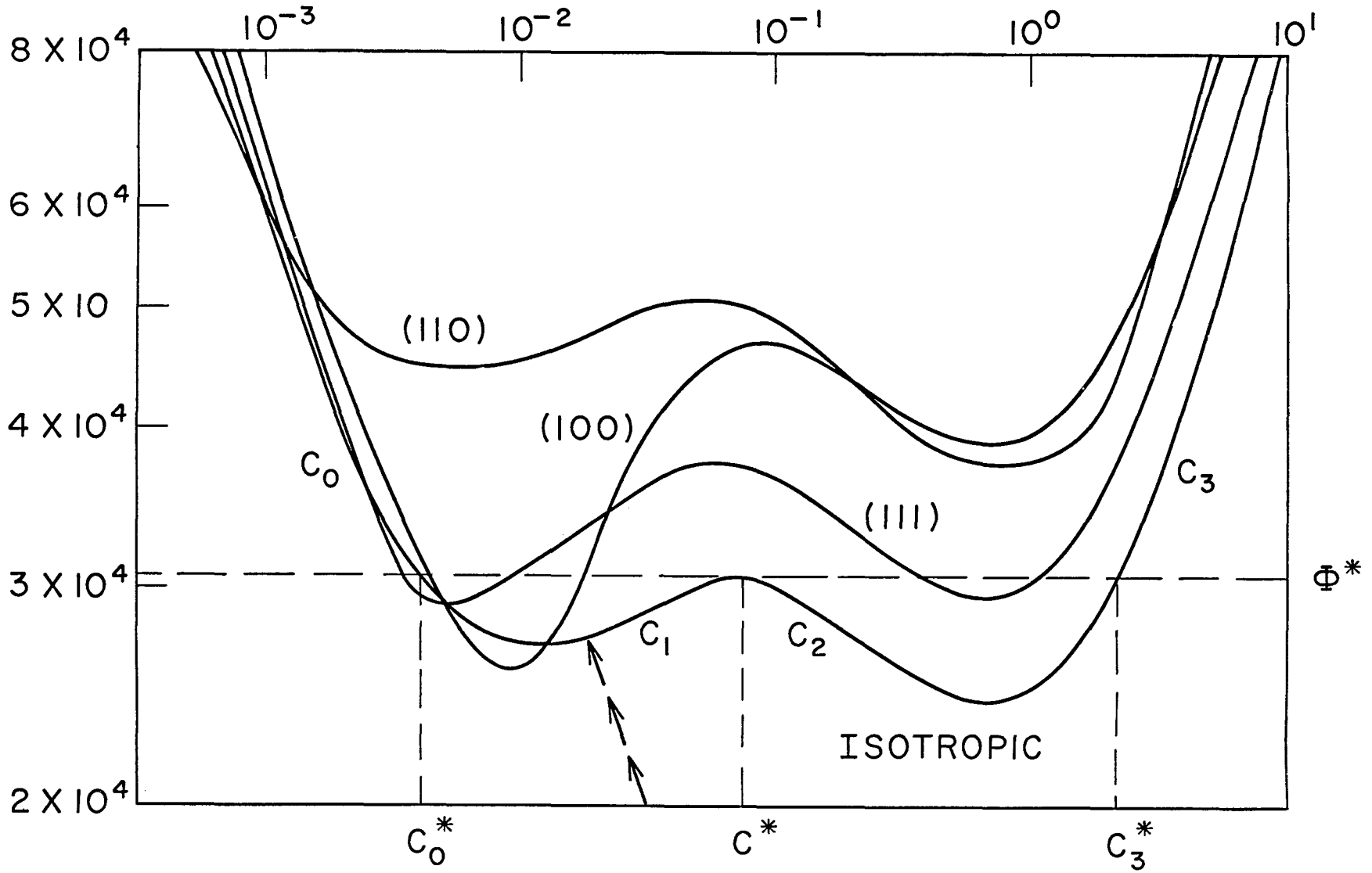
10^{-3}
10^{-2}
10^{-1}
10^{0}
10^{1}
8×10^4
6×10^4
5×10
4×10^4
3×10^4
2×10^4
(110)
(100)
(111)
C_0
C_1
C_2
C_3
Φ^*
ISOTROPIC
C_0^*
C^*
C_3^*

FIGURE 11

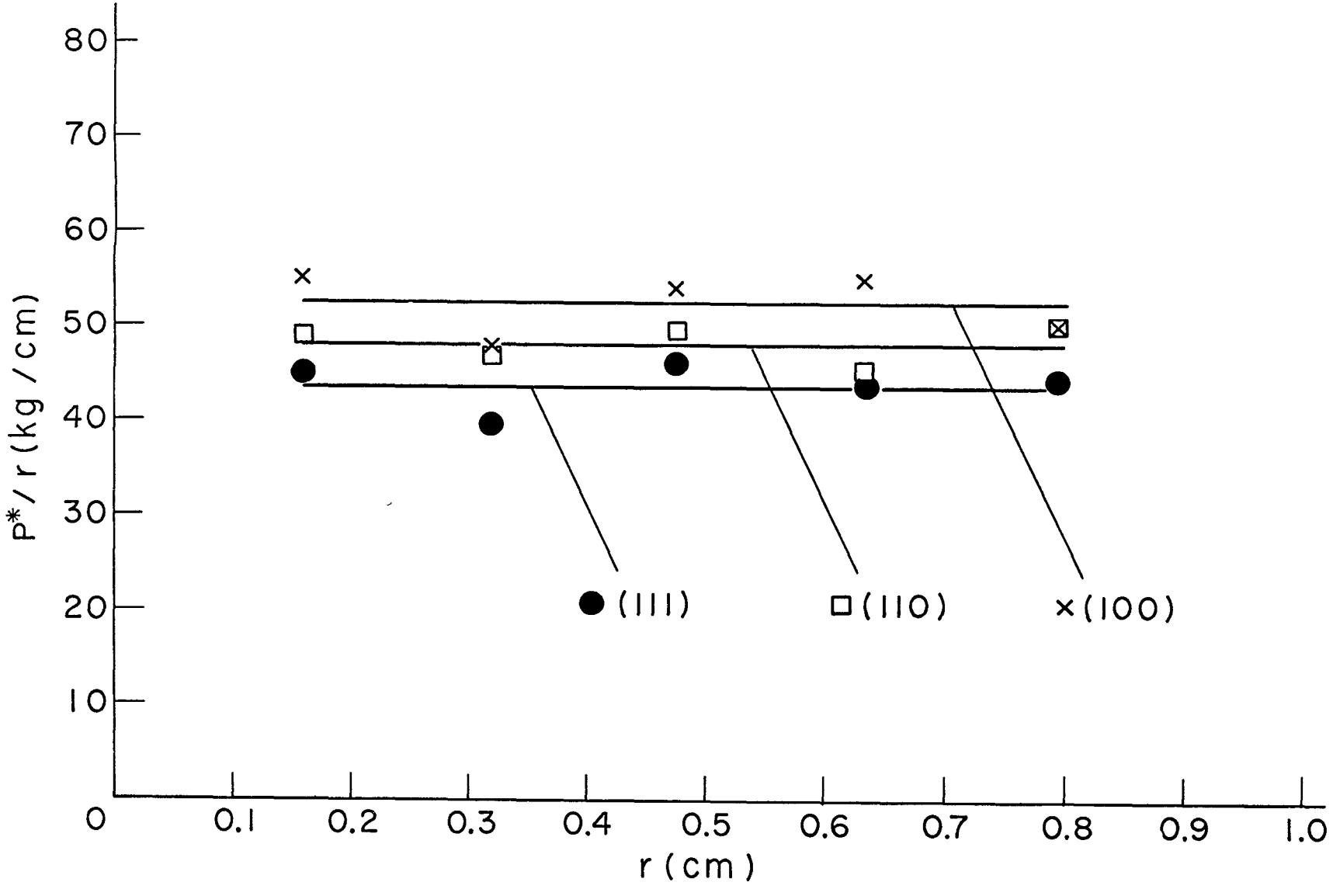
80
70
60
50
40
30
20
10
0
P*/r (kg/cm)
0.1
0.2
0.3
0.4
0.5
0.6
0.7
0.8
0.9
1.0
r (cm)
(111)
(110)
(100)

FIGURE 12